

Topological analysis and experimental control of transformations of domain walls in magnetic cylindrical nanowires

L. Álvaro-Gómez,^{1,2,3,*} J. Hurst,¹ S. Hegde,¹ S. Ruiz-Gómez,⁴ E. Pereiro,⁵ L. Aballe,⁵ J.C Toussaint,⁶ L. Pérez,^{2,3} A. Masseboeuf,¹ C. Thirion,⁶ O. Fruchart,¹ and D. Gusakova^{1,†}

¹*Univ. Grenoble Alpes, CNRS, CEA, Grenoble INP, SPINTEC, 38000 Grenoble, France.*

²*IMDEA Nanociencia, Campus de Cantoblanco, 28049 Madrid, Spain.*

³*Dpto. de Física de Materiales, Universidad Complutense de Madrid, 28040 Madrid, Spain.*

⁴*Max Planck Institute for Chemical Physics of Solids, 01187 Dresden, Germany.*

⁵*Alba Synchrotron Light Facility, CELLS, 08290 Cerdanyola del Vallès, Barcelona, Spain.*

⁶*Univ. Grenoble Alpes, CNRS, Institut Néel, 38000 Grenoble, France.*

(Dated: March 25, 2024)

Topology is a powerful tool for categorizing magnetization textures, highlighting specific features in both 2D systems, such as thin films or curved surfaces, and in 3D bulk systems. In the emerging field of 3D nanomagnetism within confined geometries, the contributions from both volume and surface must be considered, requiring appropriate topological analysis to obtain a complete view of the system. Here, we consider domain walls in cylindrical magnetic nanowires to illustrate the use of topological invariants. We begin with micromagnetic simulations of domain wall transformation under the stimulus of an (Ersted field, tracking bulk and surface topological signatures, and analyzing the interplay between multiple micromagnetic objects. For instance, the extensive analysis allowed us to highlight mechanisms of domain wall type conversion from topologically non-trivial to trivial states, a phenomenon disregarded in previous studies. Additionally, we provide experimental evidence of the transient states predicted to occur during the dynamical process.

INTRODUCTION

Topology has been for long a helpful approach to categorize nematic, magnetic and other physical textures [1]. In magnetic thin films and nanostructures, this classification includes domain walls (DWs), vortices/antivortices, and skyrmions/antiskyrmions. The emerging field of 3D nanomagnetism introduces additional magnetization textures, including Bloch points, vortex loops, hopfions, and bobbers, among others [2]. Topological invariants allow categorization of vector fields corresponding to each magnetic texture from the viewpoint of the possibility of continuous deformation. In 3D nanomagnetic finite size systems, in contrast to flat films, calculation of topological invariants involves distinct mathematical formalisms for the volume and for the surface, making analysis of a system as a whole difficult. This raises the question of how topological invariants of two sub-spaces are connected and whether it may be quantified for any type of transformations of the magnetization texture.

DWs in cylindrical nanowires made of magnetically soft materials represent an almost textbook case for investigating 3D nanomagnetism in finite size systems. Nanowires exhibit geometrical rotation invariance and under some conditions, DWs may be considered as nearly one dimensional in order to reduce complexity. However, when the diameter exceeds approximately seven times the dipolar exchange length (*i.e.* up to a few

tens of nanometers), complex 3D magnetization textures may develop [3]. The moderate dimensions of these structures allow for accurate micromagnetic simulations, and experiments are feasible using electrodeposition as a versatile growth method for high quality nanomaterials [4]. Two types of DWs topologies exist in such wires, both energetically stable and with very similar energy: the Bloch-Point-Wall (BPW) and the Transverse-Vortex-Wall (TVW) [3, 5–7]. Experimental observations have demonstrated that these DWs can dynamically change topology under the application of a sufficiently large stimulus, either a longitudinal applied magnetic field [8] or a charge current inducing an (Ersted field [9]. Simulations conducted under quasi-static conditions (with high damping $\alpha = 1$, and moderate driving force) reveal the basics of the underlying microscopic phenomenon, which involves the annihilation and nucleation of the Bloch point and of a pair of surface vortex/antivortex (V/AV). Notably, even when the initial and final states have the same topology, an empirical rule has been proposed linking 2D and 3D topological numbers to account for this process [10]. In this report, we extend and generalize the topological rule for more complex transformations, which are experimentally relevant and involve multiple topological objects under various stimuli or damping conditions. We theoretically quantify non-trivial transient states and provide experimental proof of their existence. We also demonstrate that it is possible to predictably convert the topology of a DW from BPW to TVW or vice-versa.

* laura.alvaro@ucm.es

† daria.gusakova@cea.fr

METHODS

Micromagnetics

Micromagnetic simulations were conducted with *feeLLGood* software [11–14], a home-made micromagnetic code based on finite-element methods. This code enables the accurate modeling of curved systems by discretizing the system into a mesh made of tetrahedrons. The *feeLLGood* software solves the Landau-Lifshitz-Gilbert (LLG)-Slonczewski equation, which takes into account the effect of the spin transfer, if relevant [15–17]. Here, we focus on the key role of the current-induced Oersted field which is specifically important in cylindrical systems and is crucial for DW dynamics in nanowires [18]. Thus, we intentionally disregard spin-transfer torques, and the time evolution of the unit magnetization vector \mathbf{m} reads:

$$\dot{\mathbf{m}} = -\gamma_0 \mathbf{m} \times \mathbf{H}_{\text{eff}} + \alpha \mathbf{m} \times \dot{\mathbf{m}} \quad (1)$$

where $\gamma_0 = \mu_0 |\gamma|$ [19] is the gyromagnetic ratio, α is the Gilbert damping coefficient, and \mathbf{H}_{eff} is the effective field acting on the system (sum of Oersted field, anisotropy, exchange, magnetostatics). The expression for the Oersted field in cylindrical coordinates reads $\mu_0 \mathbf{H}_{OE} = \mu_0 J \rho \hat{\boldsymbol{\phi}}/2$, with J for current density amplitude.

System considered

We consider cylindrical magnetic nanowires homogeneously made of Permalloy ($\text{Fe}_{20}\text{Ni}_{80}$). A schematic of this system, along with cylindrical coordinate axes, is depicted in FIG. 1a. The wire diameter is 90 nm, for which both types of DWs have been predicted by simulation [5, 6] and later confirmed experimentally [20, 21]. In order to mimic an infinite wire, the magnetic charges at the wire ends were removed numerically. The following material parameters were used: spontaneous magnetization $M_s = 8 \times 10^5$ A/m, zero magnetocrystalline anisotropy, and exchange stiffness $A = 1.3 \times 10^{-11}$ J/m. The resulting dipolar exchange length $\Delta_d = \sqrt{\frac{2A}{\mu_0 M_s^2}}$ is 5.6 nm. The mesh size used was 4 nm. Finally, we considered two damping coefficients, either a moderate damping situation with $\alpha = 0.1$ or a high damping situation with $\alpha = 1$. Magnetization dynamics is driven by a homogeneous charge current flowing along the wire axis z , resulting in an analytically-calculated radially-dependent Oersted field exerting a torque on magnetization. A step-like current density is applied to the system, with the starting point being the relaxed configuration of a BPW at rest, *i.e.*, with no current. While there exist four degenerate instances of BPWs at rest, differing in head-to-head versus tail-to-tail domains, and the sign of circulation, the switching mechanisms are equivalent under

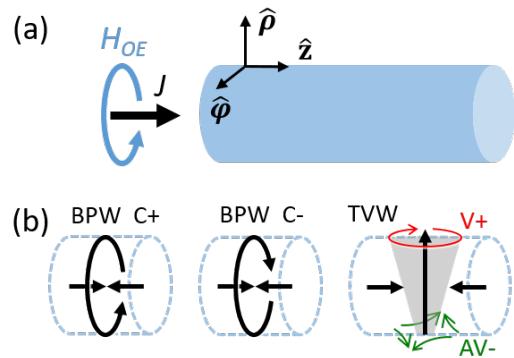


FIG. 1. (a) Schematics of the geometry of the cylindrical nanowire considered, and the current-induced Oersted field (b) Sketch of head-to-head BPW texture with positive (C+) and negative (C-) circulation, defined with respect to \hat{z} , and head-to-head TVW texture. Light arrows sketch the direction of magnetization around the surface vortex (resp. antivortex), here with positive V+ (resp. negative AV-) polarity, reflecting the sign of radial magnetization at the core of the object.

time or space symmetries. We can therefore focus on one type of initial state, without loss of generality. We consider head-to-head domains and positive initial circulation subjected to an Oersted field pulse with negative circulation in this manuscript. The DW width may be followed throughout the switching process by monitoring the Thiele wall parameter, which is defined as:

$$\Delta_T = \frac{2S}{\int (\partial_z \mathbf{m})^2 dV}, \quad (2)$$

where S is the cross-sectional area of the nanowire.

Micromagnetic singularities tracking

The BPW is characterized by magnetization curling around the wire axis (FIG. 1b). Consequently, magnetization remains largely parallel to the wire surface at all places. As these surface boundary conditions do not allow a continuous vector field to map the bulk, a magnetic singularity called the Bloch point is located at the core of the DW [22, 23]. The TVW is characterized by a component of magnetization transverse to the wire axis (FIG. 1b), with two loci having full radial magnetization at the wire surface, one outward and one inward. When the wire diameter exceeds approximately seven times Δ_d [3], magnetization tends to curl around these loci, reminiscent of V/AV patterns. While Bloch points are true micromagnetic singularities [22, 23], vortices and antivortices are not, as the vector field for magnetization in these regions remains continuous. Nevertheless, in the following, we will also refer to the latter as (surface) singularities for simplicity of vocabulary. This comes in analogy with the situation of an XY two-dimensional vector field

derived from the unit vector for the tangential component of magnetization at the surface of the wire.

The occurrence of one or the other type of singularities uniquely defines the topology of a given DW. Therefore, it is convenient to monitor them to analyze DW dynamics and possible transformations, which may involve a larger variety of situations in the transient state than at rest. To do so, we use our in-house post-processing tool for singularity tracking, developed specifically for tetrahedron-based finite elements and inspired by vector fields metrics and critical points analysis applied to computer visualization [24]. The output lists all singularities, along with their type and coordinates. Critical point classification consists of calculating the Jacobian matrix near the critical point and analyzing its eigenvalues. This mathematical procedure is applied separately in two and three dimensions. Critical points are sorted into several categories according to the sign of real and imaginary parts of the eigenvalues. Thus, on the wire surface, we obtain a spiral-type solution for the vortex and a saddle-type solution for the antivortex. In the volume of the wire the head-to-head Bloch Point corresponds to the spiral-saddle-in-type solution, whereas the tail-to-tail Bloch Point corresponds to the spiral-saddle-out-type solution.

Experimental methods

Permalloy ($\text{Fe}_{20}\text{Ni}_{80}$) cylindrical nanowires were synthesized using template-assisted electrochemical deposition. Nanoporous anodic aluminum oxide (AAO) templates were prepared by hard anodization of Al disks (Goodfellow, 99.999% in purity) in a water-based solution of oxalic acid (0.3 M) and ethanol (0.9 M), applying 140 V of anodization voltage at 0°C to 1°C for 2.5 h. The remaining Al was etched with an aqueous solution of CuCl_2 (0.74 M) and HCl (3.25 M), the oxide barrier was removed and the pores opened to a final diameter of 120 nm with H_3PO_4 (5 % vol.).

The growth conditions were similar to those described in [25]. After the electrochemical growth, the AAO templates were dissolved in H_3PO_4 (0.4 M) and H_2CrO_4 (0.2 M). Then, the nanowires were dispersed on 20 nm thick Si_3N_4 windows to allow for transmission microscopy. Nanowires were contacted electrically using laser lithography in order to allow the injection of high-frequency electric pulses, resulting in resistivity values of approximately $20 \mu\Omega \cdot \text{cm}$. To prevent sample oxidation and to enhance thermal dissipation to the Si_3N_4 , a 20 nm thick layer of Al_2O_3 was deposited on the device via Atomic Layer Deposition (ALD). Additionally, a 100 nm layer of Al was deposited on the backside of the substrate.

The wires were imaged using X-ray Magnetic Circular Dichroism (XMCD) coupled to Transmission X-Ray

Microscopy (TXM) [26] at the MISTRAL beamline of ALBA Synchrotron. The photon energy was set to the Fe L_3 absorption edge, and the X-ray incidence was set 10° off the normal to the nanowire axis, in order to be sensitive to both axial and azimuthal magnetization components. Series of about 64 images per X-ray polarization were acquired and drift-corrected prior to averaging in order to increase the signal-to-noise ratio without compromising spatial resolution. If not initially present, DWs were nucleated by applying, when on the TXM stage, a 10 ns-long pulse of current density with an amplitude of $1 \times 10^{12} \text{ A} \cdot \text{m}^{-2}$.

TOPOLOGICAL ANALYSIS DURING THE BPW CIRCULATION SWITCHING

BPWs exist with either positive or negative circulation (see FIG. 1), which we denote as $C+$ or $C-$ depending on their sign with respect to \hat{z} (FIG. 1b). While they are energetically degenerate at rest, experiments have shown that their circulation can be switched by applying a pulse of current density above a certain current density threshold [9]. The driving force behind this is the associated Oersted field, whose sign determines the circulation of the final state. The switching mechanism was studied by micromagnetic simulations under quasistatic conditions to evidence the basics of the mechanism and a minimum energy path [10]: damping was nonphysically-high with $\alpha = 1$, and the applied current density was only slightly above the switching threshold. Here, we go beyond and examine a broader range of situations. First, we consider both high ($\alpha = 1$) and moderate damping ($\alpha = 0.1$), and a larger current density amplitude: $1.50 \times 10^{12} \text{ A} \cdot \text{m}^{-2}$, well above the threshold for switching $J_c = 0.80 \times 10^{12} \text{ A} \cdot \text{m}^{-2}$. The applied current density amplitude of $1.50 \times 10^{12} \text{ A} \cdot \text{m}^{-2}$ corresponds to an Oersted field magnitude of 42.5 mT at the periphery of the wire of 90 nm diameter.

FIG. 2 illustrates the switching process of the circulation of the BPW for both high and moderate damping, highlighting the DW width evolution in time, the longitudinal position of topological objects detected, and surface magnetization maps (see FIG. 2 caption). Starting from the configuration at rest, the circulation switching can be decomposed into four main steps. *Phase 1*: Magnetization in the domains undergoes a torque from the Oersted field, which rapidly tilts magnetization towards the azimuthal direction $\hat{\phi}$, with a final angle dependent on the amplitude of the Oersted field and the radial position. At the wire surface, this increases the angle of the DW above 180° , while the central part of the BPW remains mostly unaffected as little torque is exerted, since magnetization is largely antiparallel to the Oersted field. The DW rapidly shrinks under the action of the Oersted field (FIG. 2a). *Phase 2*: An instability process devel-

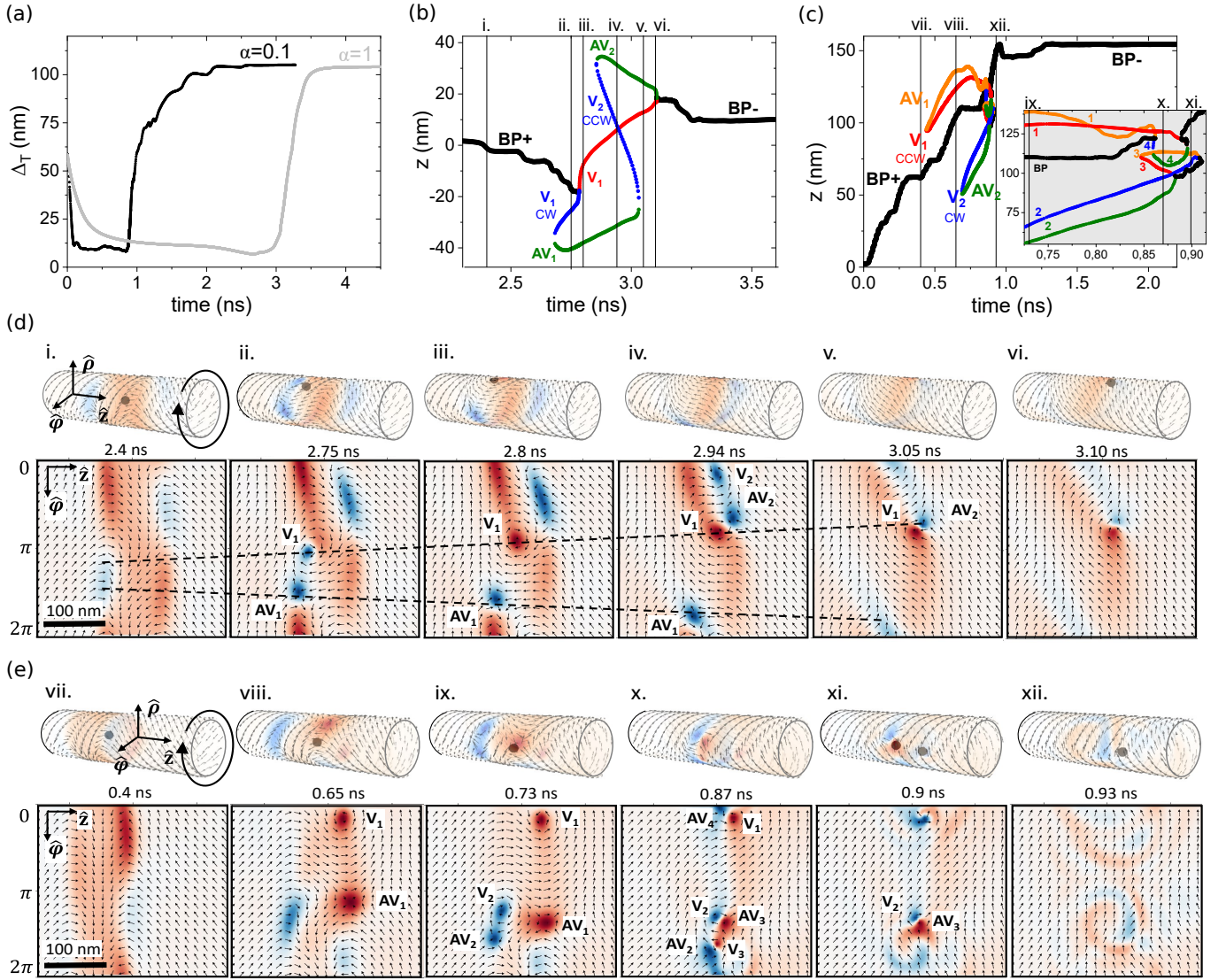


FIG. 2. Switching of circulation of a head-to-head BPW in a 90 nm-diameter homogeneous Permalloy nanowire, for damping values $\alpha = 1$ and $\alpha = 0.1$. A pulse of current density of $-1.50 \times 10^{12} \text{ A} \cdot \text{m}^{-2}$ is applied in a step-like manner at $t = 0$, resulting in a Ørsted field anti-parallel to the initial BPW circulation, with a magnitude of 42.5 mT at the surface of the wire. (a) Domain wall width Δ_T as a function of time for both damping parameters. (b) and (c): z -axis trace of the topological singularities versus time for $\alpha = 1$ and $\alpha = 0.1$, respectively. The colors indicate different topological features: black for Bloch points, red (blue) for vortices with positive (negative) polarity, orange (green) for anti-vortices with positive (negative) polarity. (d) and (e): Snapshots of the magnetic texture at selected times, for $\alpha = 1$ and $\alpha = 0.1$, respectively. The selected times are highlighted in (b) and (c), respectively. The top rows show 3-dimensional external surface views of the nanowire, while the bottom rows depict its unrolled 2-dimensional ($\hat{z} - \hat{\phi}$) cylinder surface, viewed from the outside. The color map represents the radial magnetization component, where $m_\rho = 1$ is red and $m_\rho = -1$ is blue. Dashed lines highlight the trajectories of V_1 and AV_1 .

ops, breaking the rotational symmetry. This occurs at the edges of the DW, where magnetization gradients and therefore internal torques are at their highest, and takes the form of increasing radial components of magnetization. This incubation process takes time, with no significant change in the DW width. *Phase 3*: A pair of surface V/AV may nucleate when full radial magnetization is reached at a given locus. This is followed by a complex

dynamics involving their motion around the wire periphery and interaction with a Bloch point (annihilation or re-nucleation). During most of this sequence, the DW width remains small. *Phase 4*: The topology of a BPW with circulation parallel to the Ørsted field is achieved and remains. The DW then rapidly expands, to reach a width larger than at rest.

Phases 1 and 4 are qualitatively the same, independent

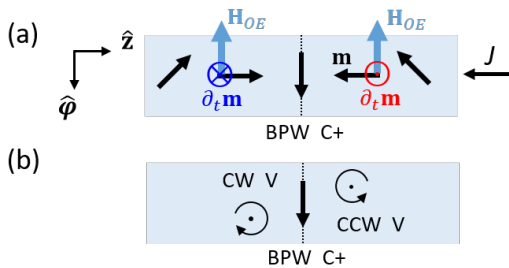


FIG. 3. (a) Simplified sketch of Ersted field induced torques on both sides from the BPW, while switching circulation from C+ to C-. (b) Illustration of vortex in-plane orientation (clockwise or counterclockwise) while switching.

of the value of current density and damping. Quantitatively, the dynamics are faster for larger current densities and lower damping, although ringing effects arise in the latter case. In the following, we focus on phases 2 and 3, which present qualitative differences. Consistent with the case of high damping and close-to-threshold current density [10], FIG. 2d and FIG. 2e show that surface singularities appear in pairs and with the same polarity. This is a continuous process, without the need for creating or annihilating a Bloch point, as shown in FIG. 2b-c. However, while in Ref.[10] only one pair of V/AV nucleated, here another one appears for $\alpha = 1$ at $t = 2.85$ ns and $z = 33$ nm, and three appear for $\alpha = 0.1$ (at 0.68 ns, 1.95 ns and 2 ns). More paths for the reversal can be explored for a larger driving force or lower damping, which is a usual micromagnetic phenomenon, as energy provided through the driving force allows the magnetization texture to explore more saddle points in the energy landscape. Nevertheless, the processes involving surface and volume singularities always obey the same rules:

- Surface singularities nucleate in the form of a pair of V/AV with the same polarity. Conversely, two such objects merging annihilate continuously.
- A Bloch point annihilates by reaching the surface through a V or AV, such as $t = 2.78$ ns for $\alpha = 1$, because all 4π orientations of magnetization must be found in its vicinity.
- Reaching the surface implies the switching of the polarity of the surface singularity, related to the head-to-head or tail-to-tail nature of the Bloch point [10]. Conversely, the merging of a V and AV with opposite polarity gives rise to the nucleation of a new Bloch point towards the inside of the wire.
- A pair of V and AV that nucleated together are not bound together, they may recombine with other AV and V.
- Two V or two AV do not nucleate nor annihilate together.

Let us provide a more quantitative insight into the first V/AV pair nucleated during the switching process. As observed in FIG. 2d, the first set of V/AV appears on the left side of the DW with negative polarity, while in FIG. 2e, it appears on the right side with positive polarity. As a matter of fact, even though the BPW is not chiral at rest, it becomes chiral during its dynamics [7, 27]. FIG. 3a illustrates this, sketching the radial torque induced on magnetization due to the Ersted field with negative circulation, on both sides of the BPW C+: dm_ρ/dt is negative on the left side and positive on the right side, consistent with the different polarity for the first V/AV pair, depending on the side of its nucleation. A dependence of the polarity of the first pair on damping is more speculative. One interpretation could be that in the quasi-static case with $\alpha = 1$, flux closure and minimization of the dipolar energy with the pre-existing $m_\rho > 1$ are promoted. Conversely, for $\alpha = 0.1$, precessional effects dominate, leading to the rapid increase of m_ρ on the right side of the DW, which quickly adds up to the pre-existing radial component.

Regarding vortices in-plane orientation with respect to the outer normal – clock-wise or counter-clock-wise – it is related to the BPW circulation as illustrated in FIG. 3b. Interestingly, vortices never change their initial in-plane orientations. Instead of this, they drift to the opposite side of the BPW to fit its final circulation after the switching. It is clearly seen in FIG. 2b for V_1 and V_2 .

The above-mentioned switching mechanism involves a complex interplay between topological objects in the bulk and at the surface. A redistribution of the topological defects is observed during the evolution of the magnetic texture, and a global picture of both bulk and surface simultaneously is necessary. This situation presents an opportunity to classify and systematize our observations using topological numbers (also called topological charge, index or winding number) [28]. In terms of formalism, here we perform our analysis strictly applied to topological defects [29]. In this sense, the Bloch point is the topological point defect (or singularity) by definition, whereas the micromagnetic vortex (antivortex) at the wire surface is not. Indeed, the vector field dimension corresponding to the vortex (antivortex) exceeds that of the spatial one. Thus, we are compelled to restrict our analysis of surface textures to the plane tangent to the wire to deal with corresponding 2D point defects. The latter implies, by definition, integer topological numbers for any type of singularity. To avoid any misleading information, the widespread calculations of topological numbers in flat films (micromagnetic vortices, skyrmions) rely on integration support modification, which deviates significantly from the initial definition of the topological invariant formula [30] (or Hopf number) and may even give non-integer values. Thus, the latter quantity (sometimes called skyrmion number) may rather be seen as a measure of the non-triviality of any vector field distribu-

TABLE I. Topological characteristics during the BPW circulation switching depicted (a) in FIG. 2b for $\alpha = 1$, and (b) in FIG. 2c for $\alpha = 0.1$. We use following notations: lower index in $()_1$ indicates the order of V/AV pair appearance in time. Red (orange) color corresponds to V(AV) of positive polarity, blue (green) corresponds to V(AV) of negative polarity. The labels (i)-(xii) correspond to particular events highlighted in FIG. 2b-c.

(a)	ω_{vol}	C_{BPW}	$\sum(\omega_{surf} \cdot p)_n$	=
i	-1	C+	-	0
ii	-1	C+	$(-1+1)_1$	0
iii	0	-	$(+1+1)_1$	2
iv	0	-	$(+1+1)_1 + (-1+1)_2$	2
v	0	-	$(+1)_1 + (+1)_2$	2
vi	-1	C-	-	0
(b)	ω_{vol}	C_{vol}	$\sum(\omega_{surf} \cdot p)_n$	=
vii	-1	C+	-	0
viii	-1	C+	$(+1-1)_1$	0
ix	-1	C+	$(+1-1)_1 + (-1+1)_2$	0
x	0	-	$(+1)_1 + (-1+1)_2 + (+1-1)_3 + (+1)_4$	2
xi	-2	C- C-	$(-1)_2 + (-1)_3$	-2
xii	-1	C-	-	0

tion. Topological invariance ensures the equivalence of two vector fields under continuous transformation, but does not guarantee any topological number conservation during the transformation process under the Ørsted field described here. Indeed, the Ørsted field driven transformations cannot be considered as continuous in the present study. Nevertheless, the classification of topological states helps to establish some empirical rules for our complex system.

For magnetic order parameter $\mathbf{m} = \{m^a, m^b, m^c\}$ the topological number of a point defect in volume is calculated using following surface integral[29]:

$${}^3w = \frac{1}{8\pi} \int_{\partial V} \epsilon_{abc} m^a dm^b \wedge dm^c, \quad (3)$$

where \wedge is for the wedge product of differential forms on the ∂V surface and ϵ_{abc} is for Levi-Civita symbol. In Cartesian coordinates $\{a, b, c\} = \{x, y, z\}$ Eq.3 simplifies to

$$w_{vol} = \frac{1}{4\pi} \int_{\delta V} [I_x dy \wedge dz + I_y dz \wedge dx + I_z dx \wedge dy], \quad (4)$$

with $I_x = \mathbf{m} \cdot (\partial_y \mathbf{m} \times \partial_z \mathbf{m})$, $I_y = -\mathbf{m} \cdot (\partial_x \mathbf{m} \times \partial_z \mathbf{m})$, $I_z = \mathbf{m} \cdot (\partial_x \mathbf{m} \times \partial_y \mathbf{m})$. It yields $w_{vol} = +1$ for the tail-to-tail configuration and $w_{vol} = -1$ for the head-to-head configuration of the Bloch point, independently

on circulation $C+$ or $C-$. For in-plane magnetic order parameter $\mathbf{m} = \{m^a, m^b\}$ on a surface, the topological number is calculated using the following closed curve Γ integral[29]

$$w_{surf} = \frac{1}{2\pi} \int_{\Gamma} m^a dm^b - m^b dm^a, \quad (5)$$

which gives $w_{surf} = +1$ for the vortex type configuration and $w_{surf} = -1$ for the antivortex type configuration. By definition these values do not take into account vortex(antivortex) polarities p with respect to the external normal which are related to the distribution of magnetic charges at the wire surface. Thus it is more relevant to analyze the following quantity $w_{surf} \cdot p$.

TABLE Ia and TABLE Ib summarize the topological numbers found at each time step denoted by a letter in FIG. 2b-c, *i.e.*, for $\alpha = 1$ and $\alpha = 0.1$, respectively. Even though the count of objects at play differs, we observe particular patterns. Thus, as expected, we obtain two sub-categories of states: either non-trivial numbers in volume with topologically neutral surface (i,ii,vi,vii,viii,ix,xii), or its opposite (iii,iv,v,x). Moreover, the difference $\Delta\omega = 2\omega_{vol} - \sum(\omega_{surf} \cdot p)_n$ stays unchanged during the switching process with $\Delta\omega = -1$. We obtain the same rule in other simulations considering different values of damping, current densities, and also for a very particular case of two Bloch points in the volume at the event (xi). We also simulated tail-to-tail DW configuration which again follows the rule with $\Delta\omega = +1$ and corresponding V/AV polarities to satisfy it. Such universality makes this rule very powerful in the analysis of micromagnetics in 3D confined systems, enabling the description of transformations involving different topological objects, such as it is the case here. Common mathematical formalism should rely on cobordism theory and is out of the scope of the present paper. Note that other approaches have been used in flat films implying half-integer numbers to account for topological objects in the “volume” and at the film edge [31]. Interestingly, topologically trivial states the in volume (iii), at the interface, mimic the topology corresponding to the TVW. This raises the question of whether it may be stabilized and what are the conditions.

CONTROLLED CONVERSION OF DOMAIN WALL TYPE

Until recently, it was considered that BPWs and TVWs followed their own dynamics and could not change into one another due to their different topology [5–7], unless there was a change in the material or geometrical parameters, such as in a cone-shaped wire [32]. However, this is only true for low diameter values, typically 50 nm or less, due to the prohibitive cost of exchange energy that would be involved in the transformation. The

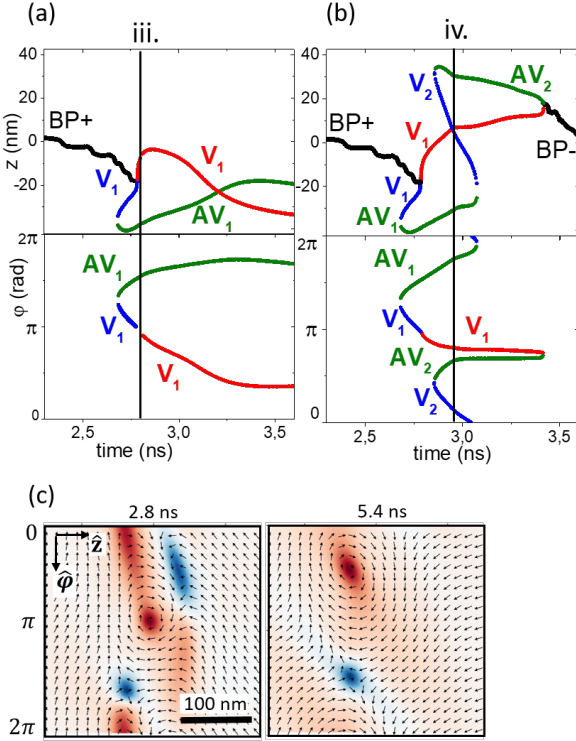


FIG. 4. Dynamics of an initially BPW state under a current density pulse of finite duration. (a-b) Time evolution of the Bloch point and V/AV pairs along the axial \hat{z} and azimuthal $\hat{\phi}$ directions. Vertical black lines indicate when the current is switched off, corresponding to times (iii) and (iv) in FIG. 2b. (c) Unrolled wire surfaces related to (a), when the current is switched off and in the final state. The color map depicts the radial magnetization m_ρ .

transformation from TVW to BPW was first reported under an applied axial magnetic field [8]. This process is promoted by the differential azimuthal speed of surface V and AV until they merge and give rise to a Bloch Point, relaxing the system into a BPW. Later on, the same transformation was described to happen under the \hat{e} field as the driving force [10]. In the following, we determine how to controllably induce the reverse transformation, from BPW to TVW, exploiting the non-BPW nature of the transient state during the circulation switching process.

Topologically trivial states in volume for the events (iii), (iv) and (v) of the TABLE Ia and FIG. 2b, i.e. when Bloch Point left the volume, suggest the possibility of stabilization of trivial magnetic texture such as TVW. At these time events, we switched off the current in our simulations and let the system relax to its final configuration. FIG. 4a-b displays the resulting temporal evolution of V/AV pairs positions along the axial \hat{z} and azimuthal $\hat{\phi}$ directions for events (iii) and (iv), correspondingly. The black vertical lines indicate when the current is switched off, at 2.8 ns in FIG. 4a and at 3 ns

in FIG. 4b. Up to that point, the plot is the same as in FIG. 2b. For the total pulse width of 2.8 ns, the final state is a TVW, whose process is also illustrated with an unrolled surface map in FIG. 4c. In contrast, for a pulse width of 3 ns, the final state is a BPW. We attribute such difference to the number of neighboring surface topological textures. Indeed, initially, a single V/AV pair favors TVW configuration stabilization, whereas a high density of V/AV pairs on the surface promotes their annihilation with Bloch Point injection into the volume.

We conducted a series of simulations to generalize the results of FIG. 4, varying the pulse width and damping parameter. We find that in all cases, if the width of the pulse is in a suitable range, a pair of V/AV leads the dynamics and remains in the system in the final relaxed state without re-introducing a Bloch Point, which is a TVW state. If the pulse is too short, the final state is a BPW with the initial circulation, only slightly translated along the axial direction. Alternatively, if the pulse is too long so that a second V/AV pair has been nucleated, the dynamics continues and ends up in a BPW with reversed circulation. A deterministic condition for BPW-to-TVW transformation seems to be that one single V/AV pair exists in the system at the time the pulse is switched off.

We have experimentally demonstrated the realization of this controlled conversion of DWs in Permalloy nanowires with 120 nm-diameter. FIG. 5a displays a TXM image at the Fe L₃ edge of a Permalloy nanowire. The corresponding XMCD image (FIG. 5b) reveals a pronounced dark and bright bipolar contrast across the wire axis. This indicates that there is locally a significant projection of magnetization along the direction transverse to the wire in a curling fashion (depicted by the yellow arrow). The light dark and bright magnetic contrast observed to the right and left sides, respectively, reveals the existence of head-to-head domains, thanks to the 10° tilt of the beam of X-rays. The combination of these two is a unique signature for a BPW with negative circulation C^- with respect to \hat{z} . Thanks to the opposite contrast arising from the neighboring domains, we can here dismiss the possibility of the central curling being due to an azimuthal domain, sometimes found in nanowires above a certain diameter approximately above 150 nm [25, 33].

In previous investigations, the switching of circulation of BPWs driven by the \hat{e} field was conducted with pulses of current of duration around 15 ns [9]. Here, we reduce the pulse duration, and as the experimental pulse duration approaches the timescale of the dynamics, we observe a change in behavior in some events. FIG. 5c displays the XMCD image after applying a 2 ns electric pulse along \hat{z} with an amplitude of $2.62 \times 10^{12} \text{ A} \cdot \text{m}^{-2}$, i.e., with \hat{e} field antiparallel to the initial BPW circulation. The magnetic contrast indicates the transformation of the BPW into a TVW. The more usual type of transformations are also observed: if a TVW is the initial state (FIG. 5e), transformation to a BPW can also be achieved

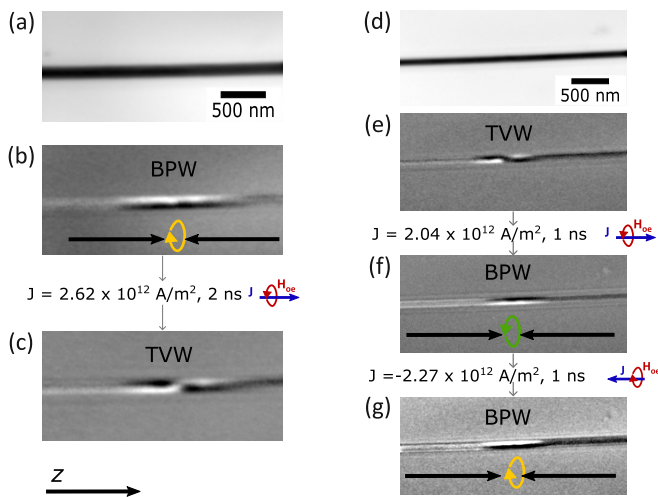


FIG. 5. X-ray imaging of current-induced DW transformations in a 120 nm-diameter Permalloy nanowire subjected to pulses of current with different duration. Each column is a different location and DW along the nanowire, with a TXM image, followed by XMCD images of the initial state (b) and (e)) and subsequent ones after current pulses (c), (f) and (g)). The black and yellow arrows indicate the direction of magnetization of the axial domains and of BPWs, respectively. **c)** Transformation to TVW after the application of a 2 ns pulse of current density amplitude $2.62 \times 10^{12} \text{ A} \cdot \text{m}^{-2}$ along \hat{z} (blue arrow), whose associated Oersted field has positive $C+$ circulation (red arrow). **f)** transformation to BPW after the application of a 1 ns current pulse of $-2.04 \times 10^{12} \text{ A} \cdot \text{m}^{-2}$ along \hat{z} , whose associated Oersted field has positive $C+$ circulation. **g)** BPW circulation switching to $C-$ after the application of a 1 ns pulse of current density amplitude $-2.27 \times 10^{12} \text{ A} \cdot \text{m}^{-2}$ along \hat{z} , whose associated Oersted field has negative $C-$ circulation.

by applying a similar pulse ($J = 2.04 \times 10^{12} \text{ A} \cdot \text{m}^{-2}$, $t = 1 \text{ ns}$), see FIG. 5f. Finally, when an electric pulse of opposite sign is applied, carrying an antiparallel Oersted field to that of the initial BPW, the resulting final state shows a BPW with reversed circulation (FIG. 5g).

These experimental observations indicate that an initial state exhibiting a BPW can lead to the transformation into a TVW or a BPW with reversed circulation when a sufficiently-short current pulse with antiparallel Oersted field is applied, and that the pulse duration matters. The transformations BPW-to-BPW and TVW-to-BPW also occur, supporting our theoretical predictions. Although the transformations are not perfectly reproducible - probably due to contributions from STT and/or Joule heating - the possibility to end up in a TVW is unambiguously proven.

CONCLUSION

In summary, we have investigated the Oersted-field induced switching of circulation of Bloch-point walls

(BPWs) in cylindrical nanowires, as a prototypical situation of a complex magnetization texture in a three-dimensional nano-object. Through micromagnetic simulations, we have predicted that the dynamical switching process involves the interplay of one or more Bloch points, considered as bulk micromagnetic singularities, with one or more pairs of surface vortex/antivortex. These surface defects can be viewed as singularities mapped onto a XY tangential magnetization field, overall obeying a 2D/3D conversion rule. This process involves redistribution of topological defects between the surface and volume of the nanowire. Furthermore, our simulations predict and experimental results confirm that transient states with a non-BPW nature can be exploited to convert BPWs into transverse-vortex walls by applying a current pulse of suitable nanosecond duration. This controlled transformation demonstrates the tunability and manipulability of complex magnetization textures in nanoscale systems, offering insights into their dynamics and potential applications in spintronics and magnetic memory devices.

ACKNOWLEDGMENTS

This work received financial support from the French RENATECH network, implemented at the Upstream Technological Platform in Grenoble PTA (ANR-22-PEEL-0015), from the French National Research Agency (Grant No. ANR-17-CE24-0017 MATEMAC-3D; Grant ANR-22-CE24-0023 DIWINA) from the Spanish MCIN/AEI/10.13039/501100011033 through Projects PID2020-117024GB-C43, TED2021-130957B-C52 and CEX2020-001039-S). S. R-G acknowledges support from the Humboldt foundation grant 1223621 and Marie Curie fellowship grant GAP-101061612. We acknowledge support from the team of the Nanofab platform (CNRS Néel institut) and from the ALBA in-house research program and MISTRAL beamline.

-
- [1] N. D. Mermin, The topological theory of defects in ordered media, *Rev. Mod. Phys.* **51**, 591 (1979).
 - [2] R. Streubel, E. Y. Tsybal, and P. Fischer, Magnetism in curved geometries, *J. Appl. Phys.* **129**, 210902 (2021).
 - [3] S. Jamet, N. Rougemaille, J. C. Toussaint, and O. Fruchart, Magnetic nano- and microwires: Design, synthesis, properties and applications (Woodhead, 2015) Chap. Head-to-head domain walls in one-dimensional nanostructures: an extended phase diagram ranging from strips to cylindrical wires, pp. 783–811.
 - [4] C. T. Sousa, D. C. Leitao, M. P. Proenca, J. Ventura, A. M. Pereira, and J. P. Araujo, Nanoporous alumina as templates for multifunctional applications, *Appl. Phys. Rev.* **1**, 031102 (2014).

- [5] H. Forster, T. Schrefl, D. Suess, W. Scholz, V. Tsiantos, R. Dittrich, and J. Fidler, Domain wall motion in nanowires using moving grids, *J. Appl. Phys.* **91**, 6914 (2002).
- [6] R. Hertel, Computational micromagnetism of magnetization processes in nickel nanowires, *J. Magn. Magn. Mater.* **249**, 251 (2002).
- [7] A. Thiaville and Y. Nakatani, Spin dynamics in confined magnetic structures III (Springer, Berlin, 2006) Chap. Domain-wall dynamics in nanowires and nanostrips, pp. 161–205.
- [8] A. Wartelle, B. Trapp, M. Staño, C. Thirion, S. Bochmann, J. Bachmann, M. Foerster, L. Aballe, T. O. Mentes, A. Locatelli, A. Sala, L. Cagnon, J. Toussaint, and O. Fruchart, Bloch-point-mediated topological transformations of magnetic domain walls in cylindrical nanowires, *Phys. Rev. B* **99**, 024433 (2019), arXiv:1806.10918.
- [9] M. Schöbitz, A. De Riz, S. Martin, S. Bochmann, C. Thirion, J. Vogel, M. Foerster, L. Aballe, T. O. Mentes, A. Locatelli, F. Genuzio, S. Le Denmat, L. Cagnon, J. Toussaint, D. Gusakova, J. Bachmann, and O. Fruchart, Fast domain walls governed by topology and cested fields in cylindrical magnetic nanowires, *Phys. Rev. Lett.* **123**, 217201 (2019).
- [10] A. De Riz, J. Hurst, M. Schöbitz, C. Thirion, J. Bachmann, J. C. Toussaint, O. Fruchart, and D. Gusakova, Mechanism of fast domain wall motion via current-assisted bloch-point domain wall stabilization, *Phys. Rev. B* **103**, 054430 (2021).
- [11] F. Alouges and P. Jaisson, Convergence of a finite element discretization for the landau-lifshitz equations in micromagnetism, *Mathematical Models and Methods in Applied Sciences* **16**, 299 (2006).
- [12] F. Alouges, E. Kritsikis, and J.-C. Toussaint, A convergent finite element approximation for landau-lifshitz-gilbert equation, *Physica B* **407**, 1345 (2012).
- [13] E. Kritsikis, A. Vaysset, L. Buda-Prejbeanu, F. Alouges, and J.-C. Toussaint, Beyond first order finite element schemes for micromagnetics, *J. Comput. Phys.* **256**, 357 (2014).
- [14] <http://feellgood.neel.cnrs.fr>.
- [15] S. Zhang and Z. Li, Roles of nonequilibrium conduction electrons on the magnetization dynamics of ferromagnets, *Phys. Rev. Lett.* **93**, 127204 (2004).
- [16] A. Thiaville, Y. Nakatani, J. Miltat, and Y. Suzuki, Micromagnetic understanding of current-driven domain wall motion in patterned nanowires, *Europhys. Lett.* **69**, 990 (2005).
- [17] M. Sturma, C. Bellegarde, J.-C. Toussaint, and D. Gusakova, Simultaneous resolution of the micromagnetic and spin transport equations applied to current-induced domain wall dynamics, *Phys. Rev. B* **94**, 104405 (2016).
- [18] A. d. Riz, *Modélisation de la dynamique de parois de domaines dans des nanofils à section circulaire*, Ph.D. thesis, Université Grenoble Alpes (2021).
- [19] L. Landau and E. M. Lifshitz, On the theory of the dispersion of magnetic permeability in ferromagnetic bodies, *Phys. Z. Sowjetunion* **8**, 153 (1935).
- [20] N. Biziere, C. Gatel, R. Lassalle-Balier, M. C. Clochard, J. E. Wegrowe, and E. Snoeck, Imaging the fine structure of a magnetic domain wall in a Ni nanocylinder, *Nano Lett.* **13**, 2053 (2013).
- [21] S. Da Col, S. Jamet, N. Rougemaille, A. Locatelli, T. O. Mentes, B. S. Burgos, R. Afid, M. Darques, L. Cagnon, J. C. Toussaint, and O. Fruchart, Observation of bloch-point domain walls in cylindrical magnetic nanowires, *Phys. Rev. B* **89**, 180405 (2014).
- [22] R. Feldtkeller, Mikromagnetisch stetige und unstetige magnetisierungsverteilungen, *Z. Angew. Physik* **19**, 530 (1965).
- [23] W. Döring, Point singularities in micromagnetism, *J. Appl. Phys.* **39**, 1006 (1968).
- [24] L. Hofmann, B. Rieck, and F. Sadlo, Visualization of 4d vector field topology, *Computer Graphics Forum* **37**, 301 (2018).
- [25] S. Ruiz-Gómez, M. Foerster, L. Aballe, M. P. Proenca, I. Lucas, J. L. Prieto, A. Mascaraque, J. de la Figuera, A. Quesada, and L. Pérez, Observation of a topologically protected state in a magnetic domain wall stabilized by a ferromagnetic chemical barrier, *Sci. Rep.* **8**, 16695 (2018).
- [26] A. Sorrentino, J. Nicolás, R. Valcárcel, F. J. Chichón, M. Rosanes, J. Avila, A. Tkachuk, J. Irwin, S. Ferrer, and E. Pereiro, MISTRAL: a transmission soft x-ray microscopy beamline for cryo nano-tomography of biological samples and magnetic domains imaging, *J. Synchro. Radiat.* **22**, 1112 (2015).
- [27] M. Yan, C. Andreas, A. Kakay, F. Garcia-Sanchez, and R. Hertel, Chiral symmetry breaking and pair-creation mediated Walker breakdown in magnetic nanotubes, *Appl. Phys. Lett.* **100**, 252401 (2012).
- [28] H.-B. Braun, Topological effects in nanomagnetism: from superparamagnetism to chiral quantum solitons, *Advances in Physics* **61**, 1 (2012).
- [29] N. D. Mermin, The topological theory of defects in ordered media, *Reviews of Modern Physics* **51**, 591 (1979).
- [30] J. H. C. Whitehead, An expression of hopf's invariant as an integral, *Proc. N.A.S.* **33**, 117 (1947).
- [31] O. Tchernyshyov and G. W. Chern, Fractional vortices and composite domainwalls in flat nanomagnets, *Phys. Rev. Lett.* **95**, 197204 (2005).
- [32] R. Hertel and J. Kirschner, Magnetization reversal dynamics in nickel nanowires, *Physica B* **343**, 206 (2004).
- [33] C. Bran, J. A. Fernandez-Roldan, E. M. Palmero, E. Berganza, J. Guzman, R. P. del Real, A. Asenjo, A. F. Rodriguez, M. Foerster, L. Aballe, O. Chubykalo-Fesenko, and M. Vazquez, Direct observation of transverse and vortex metastable magnetic domains observed in cylindrical nanowires, *Phys. Rev. B* **96**, 125415 (2017), 1705.04615v1.